Integration of responses within and across *Arabidopsis* natural accessions uncovers loci controlling root systems architecture

Ulises Rosas[a,1], Angelica Cibrian-Jaramillo[a,b,1], Daniela Ristova[a,1], Joshua A. Banta[a,c], Miriam L. Gifford[a,d], Angela Huihui Fan[a], Royce W. Zhou[a], Grace Jaeyoon Kim[a], Gabriel Krouk[a,e], Kenneth D. Birnbaum[a], Michael D. Purugganan[a], and Gloria M. Coruzzi[a,2]

[a]Center for Genomics and Systems Biology, Department of Biology, New York University, New York, NY 10003; [b]Laboratorio Nacional de Genómica para la Biodiversidad, Centro de Investigación y de Estudios Avanzados del Instituto Politécnico Nacional, Guanajuato, 36821, México; [c]Department of Biology, The University of Texas at Tyler, Tyler, TX 75799; [d]School of Life Sciences, Warwick Systems Biology, Warwick University, Wellesbourne, Warwickshire CV35 9EF, United Kingdom; and [e]Institut de Biologie Intégrative des Plantes-Claude Grignon, Unité Mixte de Recherche 5004, Biochimie et Physiologie Moléculaire des Plantes, Agro-M/Centre National de la Recherche Scientifique/Institut National de la Recherche Agronomique/SupAgro/Université Montpellier 2, 34060 Montpellier, France

Edited by Philip N. Benfey, Duke University, Durham, NC, and approved August 2, 2013 (received for review March 29, 2013)

Phenotypic plasticity is presumed to be involved in adaptive change toward species diversification. We thus examined how candidate genes underlying natural variation across populations might also mediate plasticity within an individual. Our implementation of an integrative "plasticity space" approach revealed that the root plasticity of a single *Arabidopsis* accession exposed to distinct environments broadly recapitulates the natural variation "space." Genome-wide association mapping identified the known gene *PHOSPHATE 1* (*PHO1*) and other genes such as *Root System Architecture 1* (*RSA1*) associated with differences in root allometry, a highly plastic trait capturing the distribution of lateral roots along the primary axis. The response of mutants in the Columbia-0 background suggests their involvement in signaling key modulators of root development including auxin, abscisic acid, and nitrate. Moreover, genotype-by-environment interactions for the *PHO1* and *RSA1* genes in Columbia-0 phenocopy the root allometry of other natural variants. This finding supports a role for plasticity responses in phenotypic evolution in natural environments.

GWAS | morphometrics | GxE interaction | QTL | RootScape

A long-standing debate in evolutionary biology is the relevance of phenotypic plasticity as a mechanism leading to species diversity (1). It has been argued that selection on plasticity responses to environment pressures could underlie fixed phenotypic changes between natural variants (2), providing a potentially rapid mechanism of evolutionary change (3). Thus, we tested the hypothesis that genes that enable a functional response to the environment within a population also underlie adaptive changes across natural variants. *Arabidopsis thaliana* offers ample opportunity to study genes involved in phenotypic plasticity in response to experimental laboratory perturbations, whereas its natural variants offer the opportunity to study the genetic basis for developmental variation observed in nature. We took a unique approach to integrating results from these two perspectives to uncover the molecular basis underlying individual plasticity and variation among natural variants. We focused on the root architectural system because it shows a high degree of plasticity under diverse environmental conditions (4–9). We used a quantitative phenotyping model to capture and integrate plastic changes in root system architecture in response to a range of experimental treatments within the laboratory reference accession Columbia-0 (Col-0). We next cross-referenced this plasticity space derived for an individual accession (Col-0) to the range of phenotypic differences in root architecture observed across *Arabidopsis* accessions that represent the extent of natural variation under one condition. This allowed us to identify candidate genes underlying root systems architecture using genome-wide association mapping and to test their role in individual plasticity using mutants.

Results

Integrative Characterization of Phenotypic Plasticity and Natural Variation in Root Architecture. To characterize the root plasticity "space" within an accession, we grew the *A. thaliana* laboratory strain Col-0 under a set of treatments using nutrients and hormones known to mediate different aspects of root development. This uncovered a range of plasticity within a single genotype across multiple treatments: control (KCl), auxin [Indol acetic acid (IAA)], cytokinin (CK), abscisic acid (ABA), nitrate (KNO_3), and ammonium chloride (NH_4Cl) (10) (Fig. 1*A*). Next, we characterized natural variation of root system architecture in 69 genotyped *Arabidopsis* accessions (12) grown in a single environment (KNO_3) under which they exhibit a large breadth of natural phenotypic root variation (Fig. 1*B*). Root systems architecture was quantified holistically with a method (*RootScape*) that uses landmark-based morphometrics and has the advantage of being blind to the relevance of conventional morphological characters (11, 13). This method uses a 20-point landmark template that consists of a set of reference points fixed to developmental landmarks such as the base of the primary root and to points that capture plasticity to a greater degree, such as the end of the

Significance

Species display a range of plastic phenotypes that presumably have evolved as a result of adaptation to heterogeneous environments. We asked whether the genetic mechanisms that underlie adaptation across populations also determine the response of an individual plant to environmental cues in *Arabidopsis*. Using an integrative root phenotyping approach, genes that underlie natural variation in root architecture across populations were shown to control plasticity responses within an individual. Together, our results uncover a genetic mechanism underlying the phenotypic plasticity of an individual and phenotypic diversity across natural variants.

Author contributions: U.R., A.C.-J., D.R., G.K., K.D.B., M.D.P., and G.M.C. designed research; U.R., A.C.-J., D.R., J.A.B., M.L.G., A.H.F., R.W.Z., and G.J.K. performed research; M.D.P. and G.M.C. contributed new reagents/analytic tools; U.R., A.C.-J., D.R., J.A.B., A.H.F., R.W.Z., G.K., and G.M.C. analyzed data; and U.R., A.C.-J., and G.M.C. wrote the paper.

The authors declare no conflict of interest.

This article is a PNAS Direct Submission.

Freely available online through the PNAS open access option.

[1]U.R., A.C.-J., and D.R. contributed equally to this work.

[2]To whom correspondence should be addressed. E-mail: gc2@nyu.edu.

This article contains supporting information online at www.pnas.org/lookup/suppl/doi:10.1073/pnas.1305883110/-/DCSupplemental.

PLANT BIOLOGY

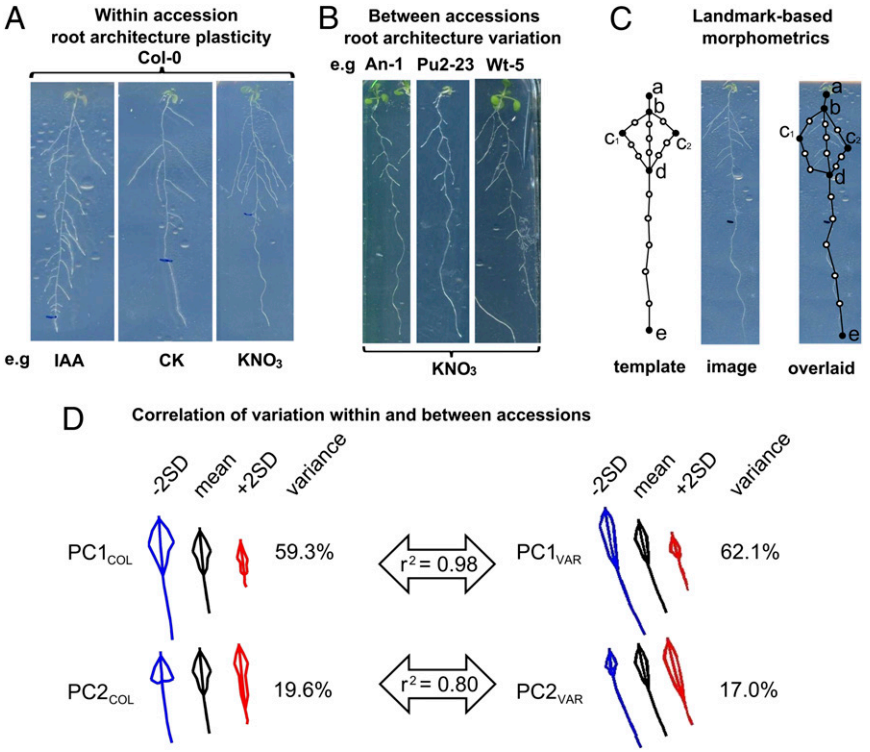

Fig. 1. Root architecture plasticity within an accession (Col-0) broadly recapitulates natural variation quantified across 69 accessions. (*A*) Root phenotypes of Col-0 plants were grown under five conditions: IAA, CK, ABA, KNO_3, and NH_4Cl plus a control (KCl); roots of three treatment conditions are shown. (*B*) Root variation between 69 accessions grown under one condition (KNO_3). (*C*) Landmark template to capture the root system architecture (11). Primary landmarks (black circles) are defined according to corresponding features in all roots; secondary landmarks (white circles) are evenly spaced between primary landmarks (11). (*D*) Two PCs capture more than 75% of the variation both within Col-0 (PC_{COL}) and between accessions (PC_{VAR}). $PC1_{COL}$ and $PC2_{COL}$ have high correlation to $PC1_{VAR}$ and $PC2_{VAR}$, respectively. $PC1_{COL}$ is mainly a size effect, whereas $PC2_{COL}$ captures mainly root allometry, the length and distribution of lateral roots long the primary root. SD, standard deviation.

primary root, the widest lateral roots, and the end of the lateral roots. Intermediate points are added evenly between the fixed landmarks. In this way the template captures the main features of root architecture as an integrated system (11) (Fig. 1*C*).

To create a framework to compare natural variation and plasticity responses, we used data from the landmark-based morphological root models and ran Principal Component Analyses (PCA). The resulting PCs uncovered the main trends of phenotypic plasticity in roots of the laboratory reference accession Col-0 (PCA_{COL}) and among the *A. thaliana* natural VARiants (PCA_{VAR}). In both root models (PC_{COL} and PC_{VAR}), PC1 and PC2 covered more than 75% of the variation in root systems architecture (Fig. 1*D*). $PC1_{COL}$ captures a size effect; $PC2_{COL}$ is an orthogonal axis to $PC1_{COL}$ and therefore captures a type of variation unrelated to size. Thus, $PC2_{COL}$ seems to capture the proportion of the primary root that contains visible lateral roots, in other words, the distribution of lateral roots in the proximal–distal axis regardless or root size (Fig. 1*D*). Similarly, a PCA of the VAR space across 69 natural *Arabidopsis* accessions captures a size-effect trend of the variation ($PC1_{VAR}$) and the lateral root allometry effect ($PC2_{VAR}$). Overall, the PC analyses suggest that the variation captured within an individual accession (PC_{COL}) is similar to the range of variation observed in natural accessions (PC_{VAR}) under our growth conditions (Fig. 1*D*). This suggests a shared genetic mechanism controlling both phenotypic plasticity and natural variation, which would imply an important role of plasticity in adaptive change.

The similarity of variation in root systems architecture observed between the plasticity space of Col-0 and across the natural accessions—($PC1_{COL} \sim PC1_{VAR}$) and ($PC2_{COL} \sim PC2_{VAR}$)—allowed us to use these PC axes as phenotypic metrics to perform quantitative comparisons. We projected the PC values for both datasets COL and VAR into the $PC1_{COL}$ and $PC2_{COL}$ axes (reference plasticity space) (Fig. 2). Surprisingly, the laboratory reference accession Col-0 (Fig. 2 *A* and *B*, blue bar), which has been historically selected for other purposes, localized roughly to the middle of the phenotypic axes of both PCs, corresponding in root phenotype to a "mean accession" relative to the other natural variants (Fig. 2 *A* and *B*, gray and blue bars). However, the treatments (Fig. 2 *A* and *B*, red bars) expanded the phenotypic breadth of Col-0, pushing its plasticity mainly toward the higher ends of the PC_{COL} axes, relative to the mean. This distribution suggests underlying developmental constraints for the plasticity to explore the lower end of the PC_{COL} space. We tested this using other *Arabidopsis* accessions and found that their plasticity is mostly directed toward the higher end of the PC axis (i.e., $PC2_{COL}$) (Fig. S1). $PC2_{COL}$ captures the distribution of the lateral roots on the primary roots. The lower end shows a narrower distribution on a range of accessions (i.e., Tamm-27) and Col-0 plasticity phenotypes (i.e., CK). The absence of phenotypes with lower $PC2_{COL}$ might reflect a bias of our selected treatments.

The projection onto the $PC1_{COL}$ and $PC2_{COL}$ phenotypic spaces (Fig. 2 *A* and *B*) also allowed us to establish that the distribution of Col-0 phenotypes resulting from experimental treatments (Fig. 2 *A* and *B*, red bars) covers ~50% of the distribution of phenotypes exhibited by the natural accessions along $PC1_{COL}$ and ~65% of the distribution in $PC2_{COL}$ (Fig. 2 *A* and *B*, gray and blue bars). We performed the reciprocal analysis and projected the same datasets into the $PC1_{VAR}$ and $PC2_{VAR}$ axes ("natural variation space") obtaining similar results (Fig. S2). A pair-wise comparison of the phenotype projections showed that $PC1_{COL}$ and $PC2_{COL}$ are highly correlated to $PC1_{VAR}$ and $PC2_{VAR}$, respectively (Fig. 1*D*). Thus, the plasticity space of individual *Arabidopsis* accessions recapitulates natural variation in root architecture when exposed to distinct laboratory-induced physiological environments.

Identification of Candidate Genes Underlying Natural Variation in Root Architecture. The projections of the PC values from the natural variants into the $PC1_{COL}$ and $PC2_{COL}$ phenotypic space were next used to map genes underlying both natural variation and phenotypic plasticity. To do this, we looked for associations between the $PC1_{COL}$ or $PC2_{COL}$ phenotypes exhibited in the natural accessions and the 214,000 SNP dataset of polymorphisms in *Arabidopsis* (14). No significant genome-wide association study (GWAS) associations were identified for the $PC1_{COL}$ trait (overall root size), suggesting that size might be

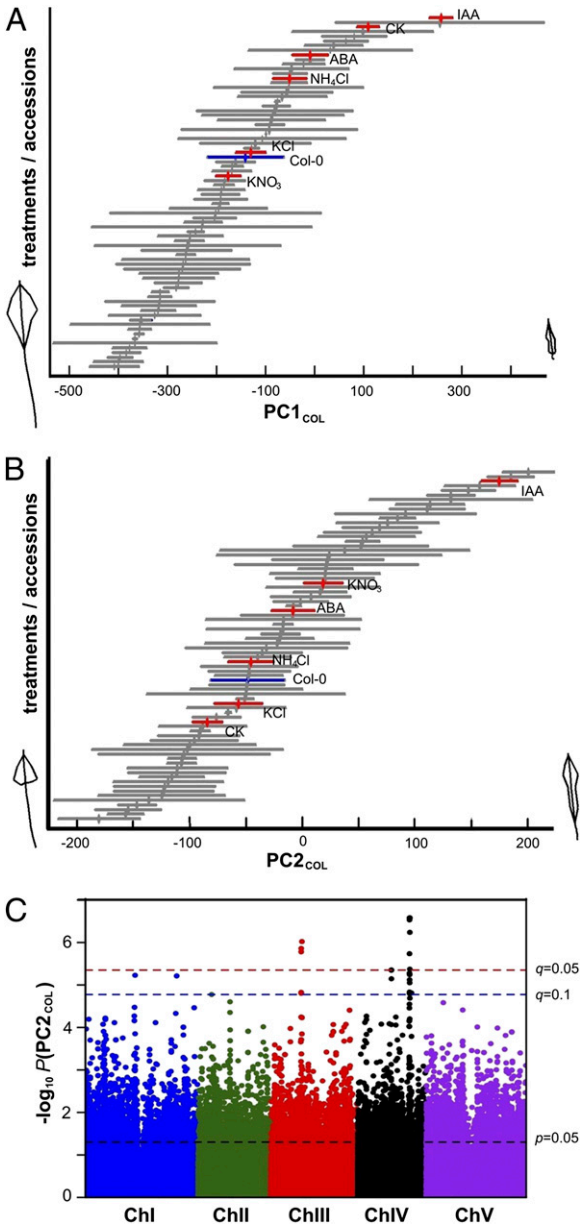

Fig. 2. Root plasticity variation within an accession (Col-0) spans a range of plasticity exhibited by *Arabidopsis* natural variants and maps to regions in chromosome III and IV. (*A* and *B*) Bars indicate SE. Red bars, Col-0 in the five treatments IAA, CK, ABA, KNO_3, and NH_4Cl and a KCl control ($n = 20$); gray bars, phenotypes of 69 *Arabidopsis* accessions grown under a single (KNO_3) condition ($n = 3$–4); blue bars, reference Col-0 accession. Morphometrics modeled root systems architecture phenotypes; those corresponding to extreme root $PC1_{COL}$ and $PC2_{COL}$ phenotypes are shown. (*C*) Manhattan plot illustrating the GWAS mapping of the $PC2_{COL}$ phenotype.

controlled by many loci of small effect. However, the $PC2_{COL}$ trait (allometry of lateral roots) revealed 12 significant GWAS associations at the false-discovery rate (FDR) level of $q < 0.05$ or 19 associations at $q < 0.1$. Most of these SNPs mapped to two genomic regions in chromosomes III and IV (Fig. 2*C*), partially overlapping regions with previously identified root morphology quantitative trait loci (QTL) (4–6, 15–18). We assumed a 5-kb window before the first and after the last significant SNPs, given that linkage disequilibrium decays more than 50% in *Arabidopsis* in that range (19). Thus, the region in chromosome (Chr) III had five SNP associations in a 212-kb interval (Chr III: 8181817–8393525 bp) containing 49 genes (Table S1, Chromosome III region). The region in chromosome IV had 18 significant SNPs in a 112-kb interval (Chr IV: 13988547–14100946 bp) containing 39 genes (Table S1, Chromosome IV region). We focused on a subset of 11 genes that each contain highly significant SNP associations (FDR: $q < 0.05$) (Table S2). Among these candidate genes is *PHOSPHATE 1* or *PHO1* (At3g23430) shown previously to play a role in inorganic phosphate loading into the xylem and aspects of root development (20, 21). Several other uncharacterized genes were also identified.

To test whether the corresponding mutant alleles show phenotypic effects for $PC2_{COL}$, we characterized the root phenotypes in mutants of six candidate genes in the chromosome III and IV regions (Fig. 3*A*). *pho1-2* (22) showed a significantly lower $PC2_{COL}$ phenotype than wild-type Col-0 (Fig. 3*A*), supporting the hypothesis that *PHO1* is one of the underlying QTL in chromosome III. A second gene that showed a significant phenotype in $PC2_{COL}$ is At4g28410 or *Root System Architecture 1* (*RSA1*). *RSA1*, a gene identified in this screen, encodes a protein that belongs to the tyrosine transaminase family, with similarity to *SUPERROOT 1* (*SUR1*; At2g20610) (23), a gene involved in glucosinolate biosynthesis from tryptophan derivatives (24).

Among other defects, the *sur1* mutant overproduces auxin because the conversion to glucosinolates is blocked, which canalizes tryptophan derivates toward auxin production, thus exhibiting extensive proliferation of lateral roots (25). We thus postulate that the *SUR1*-like gene, *RSA1*, has a redundant function to *SUR1*, and loss-of-function mutations (*rsa1-2* = At4g28410-KO) are unlikely to show strong phenotypic effects; however, overexpression alleles (*rsa1-1* = Atg428410-OX) would be expected to have an auxin deficiency-like phenotype, consistent with the phenotype of the *rsa1-1* gain-of-function mutant (Fig. 3 *A* and *B*). *rsa1-1* is a tDNA insertion mutant mapping to the 5′ UTR of A4g28410, whereas *rsa1-2* is a tDNA insertion mapping to 969 bp from the start codon, producing a predicted truncated protein of 327 amino acids (full length is 447 amino acids). To test the possible role of *RSA1* in auxin homeostasis, we obtained the genome-wide expression profile of the *rsa1-1* overexpression mutant. We found that 104 ($P < 0.001$) genes or 492 ($P < 0.01$) genes are more than 1.5-fold differentially expressed compared with the sibling wild type (Table S3). We compared the list of misregulated genes in the *rsa1-1* mutant to a list of 3,186 genes regulated by the synthetic auxin naphthalene-1-acetic acid in the root (26). We found significant overrepresentations of the intersections of auxin-regulated genes with genes misregulated in the *rsa1-1* mutant for both of our datasets ($P < 0.001$), compared with random generated gene lists of the same size (27, 28), further suggesting a *rsa1-1* role in auxin homeostasis. To further test whether expression of *RSA1* mRNA is causative to changes in root allometry, we tested whether natural variation in *RSA1* activity is correlated with changes in $PC2_{COL}$. To do this, we obtained normalized *RSA1* expression in 10 *Arabidopsis* accessions (Fig. S3) and compared them to their respective $PC2_{COL}$ phenotypes. Consistent with the result on the *rsa1-1* overexpression allele, we found a negative correlation between *RSA1* mRNA levels and the $PC2_{COL}$ phenotype (Pearson correlation: –0.55). This correlation of gene activity and phenotypic changes in $PC2_{COL}$ in the *rsa1-1* mutant, and the correlation between *RSA1* expression and $PC2_{COL}$ phenotypes in the natural accessions also supports the notion that *RSA1* (At4g28410) underlies the QTL for $PC2_{COL}$ that maps to chromosome IV.

Using the *Arabidopsis* 1,001 Genomes browser (1001genomes.org), we identified SNP positions in the *RSA1* and *PHO1* loci. For *RSA1*, the SNP at position 14051900 in chromosome IV is 348 bp upstream of the 5′ UTR. This opens the possibility that *cis*-regulatory variation at *RSA1* is driving variation in root allometry that is supported by our studies of *RSA1* expression in the *rsa1-1* mutant (Fig. 3 *A* and *B*) and in natural variants (Fig. S3). For *PHO1*, we found that the SNP at position 8388425 in chromosome III (TAIR 8 annotation) is within an exon of the coding region. Furthermore, the SNP is nonsynonymous; a cytosine

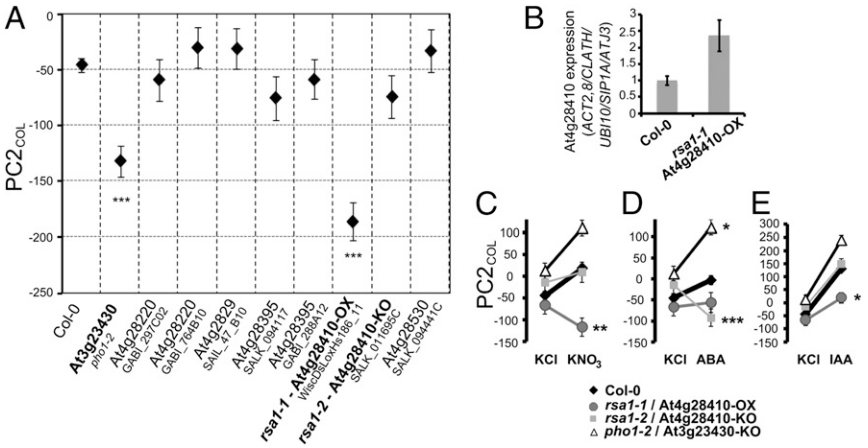

Fig. 3. Candidate genes have $PC2_{COL}$ mutant phenotypes; *PHO1*/At3g23430 and *RSA1*/At4g28410 show G × E interaction for KNO_3, ABA, and IAA conditions. (*A*) $PC2_{COL}$ values of mutant alleles for six candidate genes (n = 22–31) grown in KNO_3 media plates, compared with wild-type Col-0 (n = 36). (*B*) Quantitative PCR on the *rsa1-1* gain-of-function mutant allele (n = 3). (*C–E*) Reaction norms testing G × E interactions for IAA, ABA, CK, KNO_3, and NH_4Cl in *pho1-2*, *rsa1-1* gain-, and *rsa1-2* loss- of function mutants, respectively ($n \geq 11$). Only significant interactions (KNO_3, ABA, and IAA) are shown: $*P < 0.05$, $**P < 0.005$, $***P < 0.0005$. Error bars: SE.

at that position codes for histidine, whereas a thymine at that position codes for tyrosine. Histidine is a basic amino acid and tyrosine is an aromatic amino acid, however, the physiological ramifications of this nonsynonymous change are not clear.

Two Candidate Genes Underlying Natural Variation in Root Architecture Have Phenotypic Plasticity Responses. Genes involved in phenotypic plasticity exert environmental control over other genes that affect the phenotypic response (29). Thus, impaired activities of these genes are predicted to exhibit atypical phenotypic responses to their respective environment. To test our initial hypothesis that genes underlying natural variation can also be responsible for phenotypic plasticity, we investigated the root phenotypic response of *rsa1* and *pho1* mutant alleles to stimuli affecting the plant physiological "environment." Genotype-by-Environment interactions (G × E) in the *rsa1* and *pho1* mutants would suggest a role of *RSA1*/At4g28410 and *PHO1* in plasticity responses, as well as its associated role in natural variation. To test this, we exposed the *rsa1* mutants and the *pho1*-2 mutant allele to the five experimental treatments (IAA, CK, ABA, KNO_3, and NH_4Cl) and the control (KCl) and evaluated the resulting phenotypes along the $PC2_{COL}$ phenotypic axis. A two-way analysis of variance (ANOVA) for $PC2_{COL}$ gave a significant G × E interaction term ($P < 0.0001$) for the several treatments. For *RSA1*, significant G × E interaction effects were determined for KNO_3 ($P = 0.0031$, standardized-$\beta = -0.203$) (Fig. 3*C*) and IAA ($P = 0.0093$, standardized-$\beta = -0.177$) (Fig. 3*E*) in the *rsa1-1* overexpression mutant. ABA gave significant interactions in the *rsa1-2* ($P < 0.0001$, standardized-$\beta = -0.310$) (Fig. 3*D*). This is illustrated by the reaction norms where *rsa1-1* has a lower $PC2_{COL}$ phenotype, compared with Col-0, and the KNO_3 treatment increases the difference in the $PC2_{COL}$ phenotype of Col-0 vs. *rsa1-1*, relative to controls (e.g., KCl; Fig. 3*D*). The *rsa1-2* mutant had a lower $PC2_{COL}$ phenotype in the ABA condition compared with Col-0 (Fig. 3*D*). The *rsa1-2* mutant was not as responsive to the IAA treatment as Col-0 (Fig. 3*E*), consistent with its predicted *SUR1*-like function.

The *pho1-2* mutant showed a significant interaction in the ABA treatment ($P = 0.0228$, standardized-$\beta = 0.144$) (Fig. 3*D*), illustrated by the higher $PC2_{COL}$ phenotype of the *pho1-2* mutant compared with Col-0, specifically in our control environment (e.g., KCl). The *pho1-2* phenotype was enhanced in the presence of ABA, supporting the activity dependency between *PHO1* and ABA recently shown in stomatal responses (30). To further study the interaction of ABA and phosphate availability in the *pho1-2* mutant, we performed a combinatorial experiment in the presence or absence of ABA and phosphate. However, no significant interactions or additional phenotypes were revealed under the conditions that we tested (Fig. S4). Together, these results suggest that the role of *RSA1* and *PHO1* in mediating lateral root plasticity acts through its interplay with KNO_3, ABA, and IAA signaling. Moreover, these results show that *RSA1* and *PHO1*, candidate genes identified to be associated with natural variation in root architecture, also play roles in mediating plasticity responses within an accession *Arabidopsis*.

Finally, we tested the possibility that *RSA1* and *PHO1* natural alleles might be associated with changes in the environment using a "Landscape Genetics" approach (31), described in more detail in *Methods* and Table S4. Using environmental variables that are related to temperature and humidity (32–34), we found that none of the evaluated environmental factors (Table S4) were significantly associated with the SNP near *RSA1* in the tested accessions (Table S5). For *PHO1*, we discovered that "wet day frequency" was significantly associated with the SNP in *PHO1* ($P = 0.0027$). Specifically, the SNP allele in *PHO1* marked by a cytosine was predicted to be much less frequent in environments with fewer than 10 wet days per month compared with environments with higher wet day frequencies, whereas the SNP allele marked by a thymine was predicted to be the most frequent in environments with fewer than 10 wet days per month compared with environments with higher wet day frequencies (Fig. S5). The findings associating specific SNPs within *PHO1* with response to the environment in the field suggest future experiments to better understand this phenomenon.

Discussion

In this paper, we provide a comprehensive framework to dissect how the extent of the phenotypic response of an individual *Arabidopsis* laboratory accession relates to phenotypic plasticity intrinsic to its natural variants. Our results show that a phenotypic plasticity trait quantified in the laboratory strain Col-0 ($PC2_{COL}$) broadly recapitulates that found in natural accessions and can be used to quantify and map variation in natural *Arabidopsis* accessions (Fig. 4*A*). This intersection of individual plasticity and natural variation spaces enabled us to identify candidate genes (i.e., *RSA1* and *PHO1*) controlling variation of root allometry. Previous genome-wide studies have identified QTL for root architecture (4, 6, 15–18), some of them overlapping with our identified regions in chromosomes III and IV; but only one locus on chromosome I, *BREVIS RADIX*, has been characterized as controlling natural variation (5, 7). We now provide evidence of two more candidate genes controlling natural variation in root system architecture in *Arabidopsis* (*RSA1* and *PHO1*) and provide evidence suggesting that the environment (wet day frequency) has driven allelic variation in *PHO1* (Fig. S5).

In addition, we found that the phenotypic effects of *RSA1* and *PHO1* activities on root allometry as captured by $PC2_{COL}$ are conditional to specific environments, e.g., KNO_3, ABA, or IAA (Fig. 4*B*). Thus, a genotype-by-environment interaction mediated through the *RSA1* and *PHO1* genes determines whether the root response to ABA, IAA, and KNO_3 increases, reduces, or maintains the distribution of lateral root allometry. Moreover, these genetic and environmentally induced changes in root

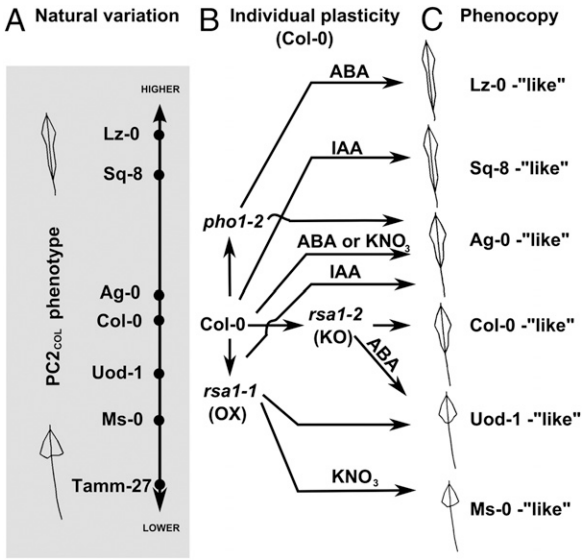

Fig. 4. The *PHO1-RSA1*-dependent G × E interaction expands the root plasticity space of Col-0 to phenocopy a range of natural accessions. (*A*) Axis representing natural variation on $PC2_{COL}$ phenotype with examples of accession's positions and root allometry phenotypes. (*B*) Treatments with KNO_3 ABA, or IAA in *rsa1-1* gain-of-function (OX) and *rsa1-2* loss-of-function (KO) mutants have contrasting effects to Col-0. (*C*) Col-0 and *rsa1* mutant alleles treated with KNO_3, ABA, or IAA phenocopy the root architecture of natural variants.

allometry in the Col-0 accession in turn phenocopies the root allometry trait of a range of natural accessions (Fig. 4*C*). This suggests that the mechanisms controlling phenotypic plasticity of root allometry Col-0 are similar to the ones controlling natural variation in *Arabidopsis* accessions. Moreover, the accessibility of the phenotypic plasticity space of an individual accession depends on the activity of genes controlling natural variation, as represented by *RSA1* and *PHO1*. These findings reopen the discussion of the relevance of phenotypic plasticity genes in natural variation and adaptive evolution (1–3, 29).

Our study also highlights a strategy for intersecting experimentally perturbed phenotypes within a laboratory strain with those observed across a panel of natural variants to uncover genetic mechanisms underlying plasticity and natural variation for any evolved trait of interest. Contextualizing root plasticity within laboratory variants and natural variation in accessions under laboratory conditions is a powerful strategy to dissect the influence of factors on plasticity typically composed of complex multigene traits, such as the impact of hormones on root system architecture. In developing a method to cross-reference the genes involved in phenotypic plasticity and natural variation, we open a window to understanding the possible mechanisms that characterize adaptive change in *Arabidopsis*.

Methods

Growth Conditions and Phenotyping. Seeds were disinfected with a solution of ethanol, bleach, and water 4:1:3 and three rinses of sterilized water. Seeds were sown on square plates of custom-made MS media (–sucrose/–nitrogen) supplemented with sucrose 0.1%, nitrogen (as indicated below), MES sodium salts 0.05% (Gibco BRL), and agar 1% (Bacto Agar BD). Plates were kept at 4 °C for 4 d in the dark and then placed vertically in a growth chamber under 22 °C, long-day 16h/8h condition at 125 $\mu mol \cdot m^{-2} s^{-1}$ light intensity (Percival Scientific). For the phenotypic characterization of accessions and mutants, the custom MS media was supplemented with 5 mM of KNO_3 and 1% of sucrose as carbon source, grown at 50 $mol \cdot m^{-2} s^{-1}$ light intensity; roots were imaged 16 d after sowing. For the IAA, CK, ABA, KNO_3, NH_4Cl, and control (KCl) treatments in Col-0 and mutants, the seeds were sown on media containing 1 mM of KCl, and seedlings were transferred to the fresh plates containing 500 nM of IAA, 500 nM of kinetin (CK), 1 μM of ABA, 1 mM of KNO_3, 1 mM of NH_4Cl, or 1 mM KCl (control), and roots were imaged 14 d after germination (4 d after transfer to treatment plates).

Plate images were obtained at 300-dpi resolution using a scanner. Landmark data and morphometric analysis were obtained using the software "Shape Model Toolbox" (12) in Matlab as described (13). Before analyzing the root variation, procrustes for translation and rotation were applied to the datasets (11, 13). This was done by aligning the datasets according to their centroid and then rotating them about the centroid to minimize the distance between corresponding landmarks; no scaling was applied. PCA was carried out on the covariance matrix to obtain the main trends of the variation (PCs), which were used as traits. Projections of other datasets were used to quantify phenotypes according to the corresponding PC_{COL}. For details on the PCA methods and projections, see refs. 13 and 35. Landmark datasets to generate the models are provided in Dataset S1.

Sampling and Statistical Tests. The phenotypic plasticity space PC_{COL} was created by growing Col-0 in the treatments described above with 20 plants per treatment. The accession data were obtained by growing three to four plants of each of the 96 Nordborg lines. Only 69 were phenotyped with the *RootScape* method (11), as the rest did not outgrow visible lateral roots under our conditions. To characterize the mutant phenotypes of candidate genes, homozygote tDNA insertion mutants and wild-type siblings were identified using primers obtained using default settings on the iSect tool (http://signal.salk.edu/tdnaprimers.2.html). Plates were sown side by side with the mutant and wild-type siblings to account for background and plate effects. The dataset consisted of $n = 239$ plants of Col-0; 36 of *pho1-2*; 23 of GABI_297C02; 25 of GABI_764B10; 24 of SAIL_47_B10; 27 of SALK_094117; 22 of GABI_288A12; 31 of WiscDsLoxHs186_11; 22 of SALK_011695C; and 22 of SALK_094441C. The projected $PC2_{COL}$ data were analyzed according to the following REML mixed model: $PC2_{COL} = \beta_{genotype} + \beta_{plate} + \varepsilon$ (Fig. 3*A*). To characterize the plasticity response of the *RSA1*/At4g28410 mutants, a minimum of 11 plants per treatment per genotype were analyzed, for a total of 291 plants. This dataset was analyzed together with the data to generate the PC_{COL} space (above). G × E interactions were tested according to the following two-way ANOVA model: $PC2_{COL} = \beta_{genotype} + \beta_{treatment} + \beta_{genotype*treatment} + \varepsilon$ (Fig. 3 *C*–*E*). To further test *pho1-2* plasticity in a phosphate-depleted environment, we custom-made MS media following the manufacturer's recipe, but also substituted the moles of $^{-}PO_4$ in KH_2PO_4 for KOH and imaged the roots 4 d after transfer to phosphate-depleted media.

Genome-Wide Association Study. After standardizing each PC_{COL} root trait to a mean of zero and a SD of 1, we performed genome-wide association mapping using the SNP database from Atwell et al. (14), which documents over 214,000 SNPs (an average of 1 SNP/500 bp) in 69 different inbred lines from the wild. We filtered the database to include only SNPs with a minor allele frequency greater than 0.10, which left 177,623 SNPs for mapping.

To account for genome-wide patterns of relatedness that can confound the results of GWAS studies (36), we used all 214,000 SNPs to construct a similarity matrix representing the proportion of loci that is identical in state between any pair of lines (K; 36). For each trait, we then separately fit the model $y = X\alpha + Zu + \varepsilon$, where y is a vector of phenotypes, X is a matrix of single-locus genotypes, α is a vector of allele effects to be estimated, Z is an identity matrix, u is a matrix of random deviates due to genome-wide relatedness (as inferred from K), and ε is a vector of residual errors. The analysis was conducted using the EMMA approach (37) in R version 3.0.1 (R Development Core Team 2013). To account for multiple simultaneous tests (because α is modeled separately for each SNP), we calculated P values that were adjusted for the genome-wide FDR (q-values) using the q-value package (38) in R (R Core Team 2013) (39).

Gene Expression Analysis. For expression analysis using quantitative PCR, the RNA extraction were carried out on roots collected from a *rsa1-2* mutant and sibling wild type at day 12, grown side by side on vertical agar plates, 5 mM of KNO_3, and 1% of sucrose at 50 $mol \cdot m^{-2} s^{-1}$ light intensity. For each of the three replicates, we pooled tissue from three roots. For assays in accessions, plants were grown in liquid media in phytatrays, and total RNA was extracted using RNeasy minikit (Qiagen). Double-stranded cDNA was synthesized by the SuperScript RT-PCR system (Invitrogen). PCR were performed using the LightCyclerFastStart DNA master^{PLUS} SYBR Green I (Roche) in a LightCycler 480 (Roche). Expression level of At4g28410 was quantified using the oligos 5′-GTGGTGATAATGAATCCTCACAAC-3′ and 5′-CCATCGGGACAAATTTATTCTCT-3′. Five standard reference genes were used to quantify relative expression: *Clathrin*/At4g24550 (5′-AGCATACACTGCGTGCAAAG-3′ and 5′-TCGCCTGTGTCACATATCTC-3′), *ACT2,8*/At3g18780,At1g49240 (5′-GGTAACATTGTGCTCAGRGGTGG-3′ and 5′-AACGACCTTAATCTTCATGCTGC-3′), *SIP1A*/At3g04090 (5′-TCCTTGTCATTGTTTAGATCCACAC-3′ and 5′-TAAATGTTTCTAAACCGGAAGAGAGTC-3′), *ATJ3*/A3g44110 (5′-TCCAACCAATTTGTCTCTTGCT-3′

and 5′-AACAAGTTTCGATGTTCCACC-3′), and *UBI10*/At4g0532 (5′-GGCCTTGTATAATCCCTGATGAATAAG-3′ and 5′-AAAGAGATAACAGGAACGGAAACATAGT-3′). All PCRs were performed with annealing of 60 °C. PCR efficiency of At4g28410 was tested with a standard curve in each plate, using four serial dilutions of a wild-type sample: 1/1, 1/10, 1/100, and 1/1000. For genome-wide expression in the *rsa1-1* mutant allele ($n = 3$) and the sibling wild type ($n = 3$), we used standard protocols from Affymetrics to amplify, label, and hybridize RNA samples to the ATH1 Affymetrics chip. Raw data were processed in MASv5.0 and two-tailed *t* test was performed in R (R Core Team 2013) (40).

Landscape Genetic Analysis. We took the significant SNP in *PHO1* (At3g23430) and the significant SNP near *RSA1* (At4g28410) and examined how they were structured on the landscape as a function of several environmental factors. We used a list of accessions and geographic coordinates of their origins (41). We intersected this list with lists of genes for which SNP genotype information is available at the two SNP loci of interest (14). We limited this list to accessions falling within the native range of *A. thaliana* in Europe and Asia (−11° to 86° E and 35° to 71° N), as estimated based on ref. 42. We then filtered this list by the "red list" and the "yellow list" of putative misidentified accessions previously flagged (41). A total of 726 accessions remained after intersecting and filtering (Fig. S5*A* and Table S5).

Separately for each SNP, we examined how the SNP was structured on the landscape as a function of temperature and humidity variables used in previous studies (Table S4). All environmental factors were at a 10 arcminute (~13 km) scale worldwide. We extracted the values of the environmental factors at the locations origin of the accessions using ArcMap version 9.3 (Esri Inc.). We then thinned the list of environmental factors to those with correlation coefficients less than |0.6| among the locations of the accessions (Table S4).

The logistic regression model was based on the logistic function $y = 1/(1 + e^{-z})$, where y is a binary dependent variable (one SNP allele or the other); and $z = \beta_0 + \beta_{1S1} + \ldots + \beta_x S_x + \beta_x + {}_1E_1 + \ldots + \beta_x + {}_yE_z + \varepsilon$, where β_0 is the intercept, $S_1 - S_x$ are the covariates to account for spatial autocorrelation (Table S4), $E_1 - E_z$ are the environmental variables, ε is the residual error, and the β terms are the corresponding regression coefficients. The analysis was performed using the lrm function of the rms package (39) in R (R Development Core Team 2013) (40).

ACKNOWLEDGMENTS. The *pho1-2* was line was kindly provided by Ives Poirier (Faculté de Biologie et de Médicine, Université de Lausanne). Rongchen Wang (Division of Biological Sciences, University of California San Diego) provided mutant lines for candidate genes. We thank Tara Moran and Nancy Francoeur for their help on Affy chips of *rsa1-1*. We thank Joan Doidy for his advice on custom media preparation. We acknowledge the feedback of Dennis Shasha and Daniel Tranchina on statistical analysis. This work was supported by National Science Foundation (NSF) Grant MCB-0929338 (to G.M.C. and K.D.B.); NSF Grant DEB-0917489 (to M.D.P.); National Institutes of Health (NIH) Grant R01 GM032877 (to G.M.C.); NIH Grant R01 GM078279 (to K.D.B.); a Human Frontier Postdoctoral Fellowship (to U.R.); a Fulbright Science and Technology award (to D.R.); a Marie Curie postdoctoral fellowship, Agence Nationale de Recherches (ANR) (NitroNet: ANR 11 PDOC 020 01); Centre National de la Recherche Scientifique (Projets Exploratoires Pluridisciplinaires Bio math Info 2012–2013: SuperRegNet) grants (to G.K.); European Molecular Biology Organization postdoctoral "A Long Term Fellowship" 107-2005; and Biotechnology and Biological Sciences Research Council Grant BB/H109502/1 (to M.L.G.).

1. Pigliucci M, Murren CJ, Schlichting CD (2006) Phenotypic plasticity and evolution by genetic assimilation. *J Exp Biol* 209(Pt 12):2362–2367.
2. Waddington CH (1953) Genetic assimilation for an acquired character. *Evolution* 7(2): 118–126.
3. Pigliucci M, Murren CJ (2003) Perspective: Genetic assimilation and a possible evolutionary paradox: Can macroevolution sometimes be so fast as to pass us by? *Evolution* 57(7):1455–1464.
4. Rauh L, Basten CB, Buckler S IV (2002) Quantitative trait loci analysis of growth response to varying nitrogen sources in *Arabidopsis* thaliana. *Theor Appl Genet* 104(5): 743–750.
5. Mouchel CF, Briggs GC, Hardtke CS (2004) Natural genetic variation in *Arabidopsis* identifies BREVIS RADIX, a novel regulator of cell proliferation and elongation in the root. *Genes Dev* 18(6):700–714.
6. Reymond M, Svistoonoff S, Loudet O, Nussaume L, Desnos T (2006) Identification of QTL controlling root growth response to phosphate starvation in *Arabidopsis* thaliana. *Plant Cell Environ* 29(1):115–125.
7. Beuchat J, et al. (2010) A hyperactive quantitative trait locus allele of *Arabidopsis* BRX contributes to natural variation in root growth vigor. *Proc Natl Acad Sci USA* 107(18): 8475–8480.
8. Ikram S, Bedu M, Daniel-Vedele F, Chaillou S, Chardon F (2012) Natural variation of *Arabidopsis* response to nitrogen availability. *J Exp Bot* 63(1):91–105.
9. Gruber BD, Giehl RFH, Friedel S, von Wirén N (2013) Plasticity of the Arabidopsis root system under nutrient deficiencies. *Plant Physiol*, 10.1104/pp.113.218453.
10. Krouk G, et al. (2011) A framework integrating plant growth with hormones and nutrients. *Trends Plant Sci* 16(4):178–182.
11. Ristova D, et al. (2013) RootScape: A landmark-based system for high-throughput screening of root architecture in *Arabidopsis* thaliana. *Plant Physiol* 161(3):1086–1096.
12. Nordborg M, et al. (2005) The pattern of polymorphism in *Arabidopsis* thaliana. *PLoS Biol* 3(7):e196.
13. Langlade NB, et al. (2005) Evolution through genetically controlled allometry space. *Proc Natl Acad Sci USA* 102(29):10221–10226.
14. Atwell S, et al. (2010) Genome-wide association study of 107 phenotypes in *Arabidopsis* thaliana inbred lines. *Nature* 465(7298):627–631.
15. Kobayashi Y, Koyama H (2002) QTL analysis of Al tolerance in recombinant inbred lines of *Arabidopsis* thaliana. *Plant Cell Physiol* 43(12):1526–1533.
16. Loudet O, Gaudon V, Trubuil A, Daniel-Vedele F (2005) Quantitative trait loci controlling root growth and architecture in Arabidopsis thaliana confirmed by heterogeneous inbred family. *Theor Appl Genet* 110(4):742–753.
17. Fitz Gerald JN, et al. (2006) Identification of quantitative trait loci that regulate *Arabidopsis* root system size and plasticity. *Genetics* 172(1):485–498.
18. El-Lithy ME, Reymond M, Stich B, Koornneef M, Vreugdenhil D (2010) Relation among plant growth, carbohydrates and flowering time in the Arabidopsis Landsberg erecta × Kondara recombinant inbred line population. *Plant Cell Environ* 33(8):1369–1382.
19. Kim S, et al. (2007) Recombination and linkage disequilibrium in *Arabidopsis* thaliana. *Nat Genet* 39(9):1151–1155.
20. Poirier Y, Thoma S, Somerville C, Schiefelbein J (1991) Mutant of *Arabidopsis* deficient in xylem loading of phosphate. *Plant Physiol* 97(3):1087–1093.
21. Hamburger D, Rezzonico E, MacDonald-Comber Petétot J, Somerville C, Poirier Y (2002) Identification and characterization of the Arabidopsis PHO1 gene involved in phosphate loading to the xylem. *Plant Cell* 14(4):889–902.
22. Delhaize E, Randall PJ (1995) Characterization of a phosphate accumulator mutant of *Arabidopsis* thaliana. *Plant Physiol* 107(1):207–213.
23. Boerjan W, et al. (1995) Superroot, a recessive mutation in Arabidopsis, confers auxin overproduction. *Plant Cell* 7(9):1405–1419.
24. Mikkelsen MD, Naur P, Halkier BA (2004) Arabidopsis mutants in the C-S lyase of glucosinolate biosynthesis establish a critical role for indole-3-acetaldoxime in auxin homeostasis. *Plant J* 37(5):770–777.
25. Seo M, et al. (1998) Higher activity of an aldehyde oxidase in the auxin-overproducing superroot1 mutant of *Arabidopsis* thaliana. *Plant Physiol* 116(2):687–693.
26. Vanneste S, et al. (2005) Cell cycle progression in the pericycle is not sufficient for SOLITARY ROOT/IAA14-mediated lateral root initiation in *Arabidopsis* thaliana. *Plant Cell* 17(11):3035–3050.
27. Katari MS, et al. (2010) VirtualPlant: A software platform to support systems biology research. *Plant Physiol* 152(2):500–515.
28. Krouk G, Mirowski P, LeCun Y, Shasha DE, Coruzzi GM (2010) Predictive network modeling of the high-resolution dynamic plant transcriptome in response to nitrate. *Genome Biol* 11(12):R123.
29. Schlichting CD, Pigliucci M (1993) Control of phenotypic plasticity via regulatory genes. *Am Nat* 142(2):366–370.
30. Zimmerli C, et al. (2012) *PHO1* expression in guard cells mediates the stomatal response to abscisic acid in *Arabidopsis*. *Plant J* 72(2):199–211.
31. Banta JA, et al. (2012) Climate envelope modelling reveals intraspecific relationships among flowering phenology, niche breadth and potential range size in *Arabidopsis* thaliana. *Ecol Lett* 15(8):769–777.
32. New M, Lister D, Hulme M, Makin I (2002) A high-resolution data set of surface climate over global land areas. *Clim Res* 21:1–25.
33. Hijmans RJ, Cameron SE, Parra JL, Jones PG, Jarvis A (2005) Very high resolution interpolated climate surfaces for global land areas. *Int J Climatol* 25(15):1965–1978.
34. Fournier-Level A, et al. (2011) A map of local adaptation in *Arabidopsis* thaliana. *Science* 334(6052):86–89.
35. Bensmihen S, et al. (2008) Mutational spaces for leaf shape and size. *HFSP J* 2(2): 110–120.
36. Yu J, et al. (2006) A unified mixed-model method for association mapping that accounts for multiple levels of relatedness. *Nat Genet* 38(2):203–208.
37. Kang HM, et al. (2008) Efficient control of population structure in model organism association mapping. *Genetics* 178(3):1709–1723.
38. Dabney A, Storey JD (2010) *qvalue: Q-Value Estimation for False Discovery Rate Control*. (Princeton University, Princeton), R package version 1.22.0. Available at www.bioconductor.org/packages/release/bioc/html/qvalue.html. Accessed August 16, 2013.
39. Harrell FE, Jr. (2013) rms: Regression Modelling Strategies. (Vanderbilt University, Nashville), R package version 3.6-3. Available at http://CRAN.R-project.org/package=rms. Accessed August 15, 2013..
40. Team RC (2013) *R: A Language and Environment for Statistical Computing* (R Foundation, Vienna).
41. Anastasio AE, et al. (2011) Source verification of mis-identified *Arabidopsis* thaliana accessions. *Plant J* 67(3):554–566.
42. Hoffman MH (2002) Biogeography of Arabidopsis thaliana (L.) Heynh. (Brassicaceae). Journal of Biogeography 29(1):125–134.